Journal of Industrial and Engineering Chemistry 144 (2025) 292–300

Contents lists available at ScienceDirect

Journal of Industrial and Engineering Chemistry

journal homepage: www.elsevier.com/locate/jiec

Full Length Article

Selective sensing of dopamine using copper hollow tube-integrated conjugated poly(arylene-ethynylene)-4 in the presence of epinephrine and norepinephrine

Jose Paul, Jongsung Kim *

Department of Chemical and Biological Engineering, Gachon University, Seongnam1342, Seongnam Daero, Seongnam-Si, Gyeonggi-do 13120, Republic of Korea

ARTICLE INFO

Keywords:
CMP-Cu-4
CMP-4
CuHT
DA
EP
NE

ABSTRACT

The Sonagashira-Hagihara coupling reaction was employed to prepare the conjugated Poly(arylene-ethynylene)-4 (CMP-4), into which copper hollow tubes (Cu-HT) were incorporated. This incorporation significantly enhanced the electrical conductivity and the selectivity of CMP-4 for dopamine (DA). The resulting composite exhibited high selectivity for DA over norepinephrine (NE) and epinephrine (EP) in a PBS-urine electrolyte. The peak current displayed a linear relationship with DA concentrations ranging from 100 to 900 nM, with limits of detection (LODs) of 17.84 and 16.03 nanomolar ($R^2 = 0.9906$). This selective DA sensing is attributed to the adsorption of the analyte on the CMP-Cu-4-GCE surface, facilitated by aromatic functionality, soft–soft interactions, Lewis basicity, and steric hindrance. Additionally, the CMP-Cu-4-GCE demonstrated remarkable sensitivity, stability, selectivity, and reproducibility in DA detection. Voltammetric results from the screen-printed electrode (SPE) using CMP-Cu-4-SPE suggest that it is a promising electrochemical probe for detecting DA in a PBS-urine solvent.

Introduction

The increasing need for precision medicine has highlighted the significance of cost-effective, portable, and easy-to-use electrochemical sensors for rapid dopamine (DA) detection. These sensors aim to customize medical recommendations based on individual factors such as genetics, metabolic profile, dietary habits, and socioeconomic status. The 1,2-dihydroxy benzenoid or catechol structure is a key component of epinephrine (EP), dopamine (DA), and norepinephrine (NE), all of which commonly exist in the brain and spinal cord of mammals [1]. DA is essential for coordinating voluntary activities, while EP and NE are primarily involved in orchestrating the body's response to stress or danger. Consequently, the quantitative determination of DA in bodily fluids can aid in diagnosing several neurological disorders. Therefore, the critical development of targeted, precise, and simple techniques for DA determination is imperative. In recent times, a range of methods have emerged specifically designed for the selective sensing of DA. These methods include liquid and gas chromatography, fluorescence, microdialysis, and electrochemistry, among others[2,3,4,5,6,7,8,9,10,11]. Recently, the electrochemical sensing method has garnered considerable interest due to its elevated sensitivity, convenience, rapidity, reproducibility, and ease of manipulation.

Conjugated microporous polymers (CMPs) are 3D semiconducting amorphous polymers distinguished by their formation of π-conjugated microporous networks through double or triple bonds[12]. Cross-coupling reactions in a kinetic irreversible process are often utilized to synthesize CMPs, resulting in a solid product having a surface area of at least 834 m^2/g, [13]. This results in a solid-state porous material that is both lightweight and hydrophobic. The exceptional physical and chemical properties of these polymers are due to the presence of conjugation, which can occur through their double, or triple bonds. These unique structures confer a diverse array of applications, including photoluminescence, catalysis, sensing platforms, battery applications, and photocatalytic hydrogen evolution[12,14,15,16,17,18,19,20,21,22,23]. Interconnected porous frameworks find diverse applications in electrochemical sensing mechanisms. The extensive presence of π conjugation within CMP networks greatly enhances charge transfer efficiency[24,25,26]. Additionally, the substantial pore size will enhance the interaction between the analyte and the surface of the CMP. Over recent years, utilizing CMP, electrochemical and fluorescence sensors were fabricated for DA, picronitric acid, and fluoride ions based on the aforementioned principles[27,28,29,30,31,32,33].

---

* Corresponding author.
E-mail address: jongkim@gachon.ac.kr (J. Kim).

https://doi.org/10.1016/j.jiec.2024.09.023
Received 18 July 2024; Received in revised form 4 September 2024; Accepted 15 September 2024

Using the solvothermal method, we synthesized a composite material consisting of a copper hollow tube (CuHT) embedded within a conjugated microporous poly(arylene-ethynylene)-4, referred to as CMP-Cu-4. This approach involved post-synthetic modification of the CuHT within the CMP-4 matrix, resulting in the formation of a conductive spherical and tubular organic–inorganic composite. This composite is designed to facilitate enhanced unidirectional charge delocalization, thereby optimizing the material's electronic properties. The research process used in this study, which included the solvothermal preparation method and non-toxic copper modification, led to a cost-effective synthesis procedure with non-leachable properties. This method ensured the precise functionality of the sensing mechanism while also adhering to eco-friendly and sustainable principles in material synthesis. The prepared CMP-Cu-4-GCE selectively senses DA in the presence of EP and NE, which are structural analogs of DA and typically oxidize at the same potential on most GCEs along with DA. The exceptional stability, sensitivity, and reproducibility indicate that the prepared CMP-Cu-4-GCE is a promising electrochemical probe for the selective sensing of DA in PBS. To evaluate the physical properties, we used XRD, Raman, SEM, and EDX techniques. For chemical characterization, we utilized methods such as FTIR and XPS. Furthermore, we examined the redox behavior of the modified glassy carbon electrodes (GCE) using cyclic voltammetry (CV) and electrochemical impedance spectroscopy (EIS).

Experimental section

Chemicals and reagents

We acquired the chemicals, reagents, and solvents from Sigma Aldrich and Duksan, using them as received without further purification. 1,3,5-tribromobenzene [$C_6H_3Br_3$], 1,4-diethynylbenzene [$C_{10}H_6$], tetrakis-triphenylphosphine)palladium [$C_{72}H_{60}P_4Pd$], hexaaminerruthenium-(III) chloride [$Ru(NH_3)_6Cl_3$] (98 %), copper iodide [CuI], toluene [C_7H_8], triethylamine [Et_3N], chloroform [$CHCl_3$], dopamine hydrochloride [$C_8H_{11}NO_2{\cdot}HCl$], potassium ferrocyanide [$K_4[Fe(CN)_6]$] (98 %), epinephrine [$C_9H_{13}NO_3$], norepinephrine hydrochloride [$C_8H_{12}ClNO_3$], aspartic acid [$C_4H_7NO_4$], oleyl amine [$C_{18}H_{37}N$] and toluene [C_7H_8], were obtained from Sigma Aldrich. Ethanol [C_2H_6O] and hydrochloric acid (HCl) were obtained from Duksan (Ansan, Republic of Korea). Phosphate-buffered saline (PBS) (10 mM, pH 7.4) and Deionized water were utilized in the voltammetric experiments.

Electrochemical probes and equipment

The voltammetric experiments employed an electrochemical technique utilizing a three-electrode setup. The working electrode consisted of a glassy carbon electrode with a surface area of 0.07 cm^2, accompanied by a coiled platinum wire acting as our counter electrode (CE), and a saturated KCl Ag/AgCl electrode serving as reference electrode (RE). In each voltammetric experiment, the glassy carbon electrode underwent polishing with 0.05 µm −sized alumina powder and subsequent cleaning with diluted ethanol and deionized water. We purchased a screen-printed electrode (SPE) from Metrohm DropSens. For the Votammetric experiments, we used Metrohm DropSens 250AT as SPE. The working electrode (WE) consisted of a gold electrode, accompanied by a platinum as counter electrode (CE), and a silver electrode serving as reference electrode (RE). Voltammetric measurements, including CV and EIS, were conducted at room temperature using the three-electrode system in WizMac WizEIS-1200 Premium voltammeter.

Voltammetric assessment of different modified GCEs

Our research group studied the selective sensing of DA towards CMP-Cu-4-GCE at a pH of 7.4, which is the typical pH range of the human body in the absence of pathological states. We assessed the voltammetric characteristics of different modified GCEs in both PBS and diluted urine-PBS solutions containing varied concentrations of DA. Additionally, we assessed the electrochemical behavior of Cu, CMP-4, and CMP-Cu-4 modified GCE towards DA in PBS. To evaluate the performance of CMP-Cu-4-GCE, we performed electrochemical characterization measurements using PBS (1 mM and pH=7.4) and PBS-urine as the electrolyte. We used 1 mM $Ru(NH_3)_6Cl_3$ and [$K_4[Fe(CN)_6]$] as a redox gauge for the scan rate experiments. We tested the impedance response of CMP-Cu-4-GCE from 0.1 to 10^6 Hz, with an amplitude of 10 mV (pH=7.4, 1 mM). For the urine-PBS solution, 5 mL of urine was combined with PBS (1 mM) to make a total volume of 100 mL.

CMP-4, Cu-HT, and CMP-Cu-4 composite preparation

A mixture of 1,3,5-tribromobenzene (49.8 mg, 0.158 mmol) and 1,4-diethynylbenzene (50 mg, 0.396 mmol) was prepared in Et_3N (2.5 mL) and toluene (5 mL) in a 50 mL glass vial[13]. The vial was purged by using gaseous nitrogen to avoid the homocoupling reaction between individual alkyne monomers. Tetrakis(triphenylphosphine)palladium (11 mg) and CuI (3.5 mg) were then added. The reaction mixture was heated to 80 °C for 72 h. After cooling to room temperature, the resulting polymer was sieved through 90 mm filter paper and washed sequentially with chloroform, water, methanol, and acetone, each wash performed four times. The CMP-4 polymer underwent thorough purification via Soxhlet extraction in methanol over 48 h, after which it was dried in an oven at 60 °C for 6 h.

CuHT was synthesized from a mixture of CuCl and Oleylamine (OLA) following established procedures[34]. Initially, 25 mg (0.25 mM) of CuCl was dissolved in 5 mL of OLA in a 100-mL amber-colored glass vial. Subsequently, the solution temperature was raised to 170 °C for 61 h with continuous stirring, resulting in the formation of a reddish-brown solution, signifying the reduction (Cu^+ to Cu^0) and precipitation of copper. The reaction temperature of the reactants was gradually reduced to room temperature (RT) without any further stirring. The obtained brown-colored mixture underwent three washes by using 30 mL of toluene, followed by 10-second sonication and centrifugation at 8000 rpm for 5 min. The collected sample was then dried in a vacuum at 60 °C and stored in an inert condition for subsequent analysis and characterization.

To synthesize the CMP-Cu-4, 25 mg of CuCl was blended with 50 mg of prepared CMP-4 in OLA (5 mL) within a 100 mL amber glass vial (Scheme 1). The mixture was thoroughly sonicated for 10 min for the dissolution of CuCl. Subsequently, the temperature of the reaction mixture was raised to 170 °C (61 h) with continuous stirring. During this process, the solution changed to a deep brown color, indicating precipitation of Cu^0 in between the CMP-4 surface. The reaction temperature was then gradually reduced to RT without further stirring. The obtained CMP-Cu-4 composite underwent three wash cycles, each involving the addition of 30 mL of toluene, 10 s of sonication, and centrifugation (8000 rpm, 5 min). This purification was repeated 4 times. Finally, the composite was dried in a vacuum oven (60 °C) for 24 h and stored in an inert condition.

Results and discussion

Physical and chemical analysis of the CMP-4 and CMP-Cu-4

The prepared poly(arylene-ethynylene) underwent functional group analysis using infrared (IR) spectroscopy. Results revealed three diagnostic peaks corresponding to doubly substituted −C≡C- stretching, aromatic bending from benzenoid ring (−C=C- bending), and the aromatic C–H stretching at 2360, 1394, and 3030 cm^{-1}, respectively (Fig. 1a). The ^{13}C NMR (solid-state) spectra revealed three distinct peaks corresponding to carbon atoms in poly(arylene-ethynylene), indicating their presence in three different chemical environments (Fig. 1b). Two highly de-shielded carbons were observed in the aromatic ring, while one shielded alkynyl carbon was found outside the aromatic ring. The

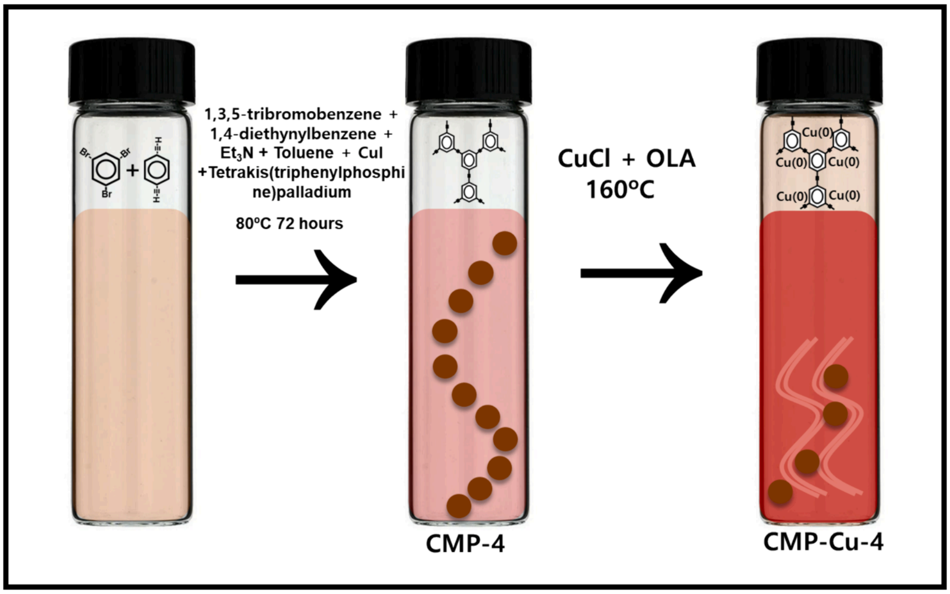

Scheme 1. Preparation of CMP-4 & CMP-Cu-4.

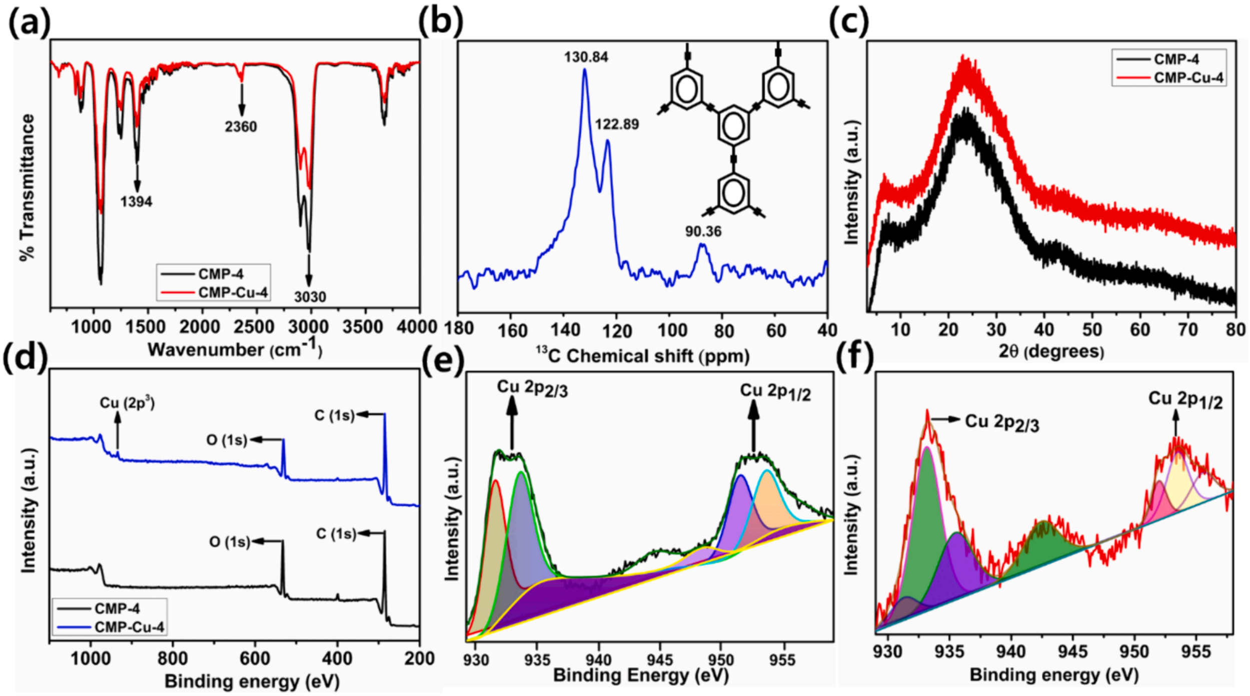

Fig. 1. (a): FT-IR spectra of CMP-4 & CMP-Cu-4, **(b)** ^{13}C solid-state NMR spectra of CMP-4, **(c)** XRD spectra of CMP-4 & CMP-Cu-4, **(d)** XPS total survey spectra of CMP-4 & CMP-Cu-4, **(e)** deconvolution spectra of Cu prepared from CuCl-OLA, and **(f)** deconvolution spectra of Cu from CMP-Cu-4.

triply bonded carbon exhibited a shift of 90.36 ppm for CMP-4, while the acetylene-bonded carbon within the aromatic ring showed shifts of 122.89 ppm. The unbonded carbon displayed shifts of 130.84 ppm.

XRD was employed to analyze the crystal phase and defect characteristics of CMP-4 (Fig. 1c). The XRD patterns spanning from 3 to 80° displayed a broad diffraction peak at θ = 20°, indicating the highly disordered nature of CMP-4. Despite CMP-4 being prepared under kinetically driven conditions, resulting in an amorphous structure. We employed a solvothermal technique to introduce copper into the structure of CMP-4 during post-modification. In the method of synthesis, oleyl amine (OLA) served as both a capping agent and solvent, enabling the reduction of Cu^+ to Cu^0 at room temperature. When the temperature reached 100 °C, the reaction produced a coloration resembling grape wine. Subsequently, Cu^0 atoms crystallized in a hollow tubular form within CMP-4 through the Ostwald ripening mechanism at 170 °C.

Raman spectroscopy was utilized for the intrinsic structure of CMP-4 and CMP-Cu-4. As depicted in Fig. S1a, the peak observed at 1350 cm^{-1} corresponds to the D-band, signifying the existence of disordered sp^2 hybridized carbon rings. Conversely, the peak at 1590 cm^{-1} corresponds to the G-band, indicating the presence of in-plane vibration of sp^2 hybridized carbon within the framework. Notably, the intensity of the G band in the composite surpasses that of the D band, suggesting a collective contribution from CMP-4 and CMP-Cu-4 peaks.

The XPS survey spectrum unveiled the presence of core–shell electronic energy levels for C(1 s) in the CMP-4 composite (Fig. 1d). Moreover, the overall survey spectrum indicated an additional peak corresponding to Cu($2p^3$) in CMP-Cu-4 (Fig. 1d). Additionally, the C(1 s) peak remained unchanged post-doping, affirming the stability of CMP-4 despite Cu integration (Fig. S2(a&b)). The deconvolution spectra of Cu (0) obtained from the CuCl-OLA reactant blend revealed peaks at 952 and 932 eV, corresponding to the Cu ($2p^{1/2}$) and Cu ($2p^{2/3}$) spin orientation, respectively (Fig. 1e). Consequently, the comparable binding energy observed for Cu(0) in the CMP-Cu-4 composite indicates that the metal maintained Cu(0) oxidation state after the copper incorporation (Fig. 1f). Similarly, compatible deconvolution spectra for C(1 s) in both CMP-4 and CMP-Cu-4 validate the chemical stability of CMP-4 following Cu integration (Fig S2 a&b). The XPS analysis of CMP-Cu-4, indicated by the C (1 s) and Cu ($2p_3/_2$) peaks, provides specific insights into the valance electronic configurations of C and Cu. The C (1 s) peak confirms the presence of carbon atoms in both sp and sp^2 hybridized states, suggesting that in CMP-4, these carbon atoms are covalently bonded to each other. Meanwhile, the Cu ($2p_{3/2}$) peak reveals an electronic configuration of [Ar] $3d^{1o}$ 4 s^1 for copper, indicating a fully occupied 3d orbital and a partially filled 4 s valence subshell. To determine the surface atomic percentages of C and Cu through XPS analysis, we first analyzed the XPS data and found that CMP-4 contains 79.46 % C (1 s) and 0.04 % Cu (2p3/2). The trace amount of copper likely comes from the reactant in CMP-4, which utilizes CuI as a cocatalyst in its synthesis. Furthermore, we identified the surface atomic percentages of CMP-Cu-4 as 82.54 % for C (1 s) and 0.6 % for Cu (2p3/2). This indicates a substantial increase in copper content in CMP-Cu-4 compared to CMP-4. Overall, the presence of alkynyl bonding in the CMP-Cu-4 network contributed to its chemical stability. In summary, the synthesis of both CMP-4 and CMP-Cu-4 was validated through comprehensive physical and chemical analyses.

Morphological characterization of the CMP-Cu-4

SEM was employed to evaluate the surface characteristics and shape of the as-synthesized CMP-4 and CMP-Cu-4. The CMP-4, appearing brown in color, was determined to comprise solid spheres of submicrometer dimensions, as illustrated in Fig. 2a. The SEM image of the CMP-Cu-4 nanocomposite displayed a hollow tubular configuration enveloped by CMP-4 spheres, indicating the successful encapsulation of CMP-4 around the CuHT (Fig. 2b&c). The average size of CMP-4 was calculated to be 1.4 µm, while for CuHT, it measured approximately 495 nm (Fig. S2(a-c)). Additionally, the elemental composition analysis via the EDAX spectrum verified that the CMP-Cu-4 composite contained 95.99 % carbon (C) and 4.01 % copper (Cu) (Fig. S4 & Table S1). Nevertheless, the lack of additional elements like nitrogen (N) in the fabricated materials affirmed the purity of CMP-Cu-4. TEM was employed to examine the external structure and flaws of CMP-4 and CMP-Cu-4 (Fig. 2d&e). The TEM images validated the SEM analysis, showing spherical CMP-4 particles with an average size of 1.4 µm. SEM and TEM images confirm that the CMP-4 spheres were observed wrapped around the CuHT, resulting in spherical and tubular structures of CMP-Cu-4. Physical and morphological examinations confirmed the presence of CuHT in between the CMP-4 framework, establishing that CMP-Cu-4 was indeed a nanocomposite.

Redox response of CMP-Cu-4-GCE towards $Fe(CN)_6^{3-/4-}$ & $[Ru(NH_3)_6]^{3+}$

The complexes $[Ru(NH_3)_6]^{3+}$ and $[Fe(CN)_6]^{3-}/^{4-}$ are well-studied probes for electrochemical research. $[Ru(NH_3)_6]^{3+}$ exhibits very high sensitivity and is often used in electrochemical studies of novel sensors. $[Fe(CN)_6]^{3-}/^{4-}$ is highly stable and provides reproducible redox cyclic voltammetry (CV) probes for electrochemical studies. In our research, we used $[Ru(NH_3)_6]^{3+}$ and $[Fe(CN)\ _6]^{3-}/^{4-}$ to evaluate the charge transfer mechanism by analyzing the log(scan rate) vs. log(current) plot. The study involved examining the kinetics of reversible single electron transfer reactions using positively and negatively charged $[Ru(NH_3)_6]^{3+}$ & $Fe(CN)_6^{3-/4-}$ at a concentration of 1 mM and a pH of 7.4. The impact of scan rate variation towards $[Ru(NH_3)_6]^{3+}$ was investigated (Fig. 3a) [35]. A strong correlation was observed between the log (scan rate) vs. log (anodic current) (R^2 = 0.9685), indicating a diffusion-controlled mechanism with a slope of 0.4085 (Fig. S5c). The reduction peak corresponding to the conversion of ferricyanide to ferrocyanide was marked at −0.033 V (Fig. 3b). A significant relationship was found between the log (scan rate) and the log (anodic current) (R^2 = 0.999), with a slope of 0.7843, affirming the dominance of adsorption in the redox mechanism (Fig. S5d).

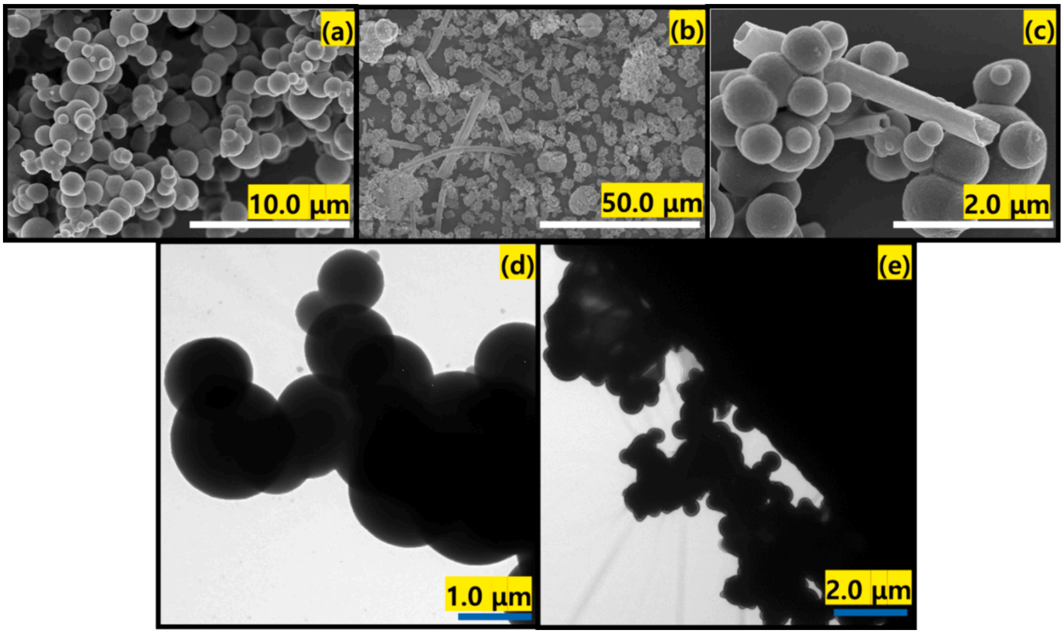

Fig. 2. **(a):** SEM image of CMP-4, **(b&c):** SEM image of CMP-Cu-4, & **(d&e):** TEM image of CMP-4 & CMP-Cu-4.

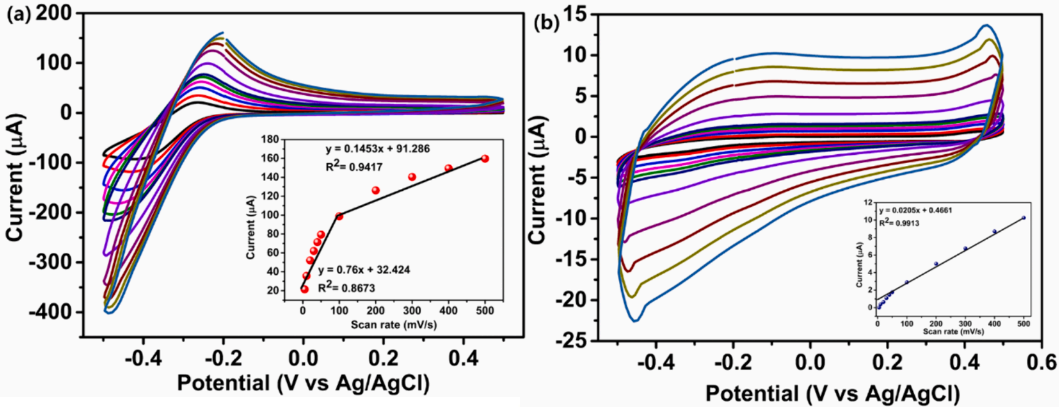

Fig. 3. **(a):** Electron transfer reactions using positively $[Ru(NH_3)_6]^{3+}$ & **(b):** negatively charged $Fe(CN)_6^{3-/4-}$.

Impedance spectra of various modified GCE

The concept of charge transfer resistance (Rct), which gauges the difficulty in transferring charge from the electrolyte to the electrode surface, is analogous to resistance. In voltammetry, Rct represents interfacial resistance between the CMP-Cu-4-GCE and PBS. Utilizing the Nyquist plot, Rct values were determined to be 635.53, 658.36, and 666.48 Ω for CMP-Cu-4-GCE, GCE (bare), and CMP-4-GCE respectively (Fig. 4a). Notably, the lesser Rct observed for CMP-Cu-4-GCE implies a more efficient electron transfer at the GCE surface and electrolyte interface.

The redox study of CMP-Cu-4-GCE towards DA in human urine and PBS mixture

The redox process of DA on a GCE is characterized as apparent redox, unique from the EP oxidation. As per the Electron Transfer-Coupled Chemical (ECC) mechanism, pH-dependent voltammetric sensing involves an oxidation reaction of a 1,2-dihydroxy benzene ring on modified electrodes, forms the o-quinone (OQ) [36,37]. The subsequent step involves the OQ undergoing intramolecular cyclization and internal oxidation–reduction, leading to the formation of leucoaminochrome (LAC). Significantly, the rates of cyclization differ for each catecholamine at pH=7.4 (k_{NE}=0.98 + 0.52 s^{-1}, k_{DA}=0.13 + 0.05 s^{-1}, and k_{EP}=87 + 10 s^{-1}). Subsequently, LAC initiates a homogeneous reaction with other OQ, leading to an oxidation to form amino chrome (AC), while the OQ reverts to its 1,2-dihydroxy benzene form AC ($E_{1/2}$ = −0.207 V vs Ag/AgCl (sat KCl)). The presence of β-hydroxy groups in EP and the methyl group in NE leads to variations in the rate constants of the cyclization reaction. These differences enable the selective sensing of DA. Also, the greater steric hindrance of NE and EP compared to DA contributes to their reduced adsorption on appropriate CMP-Cu-4-GCE.

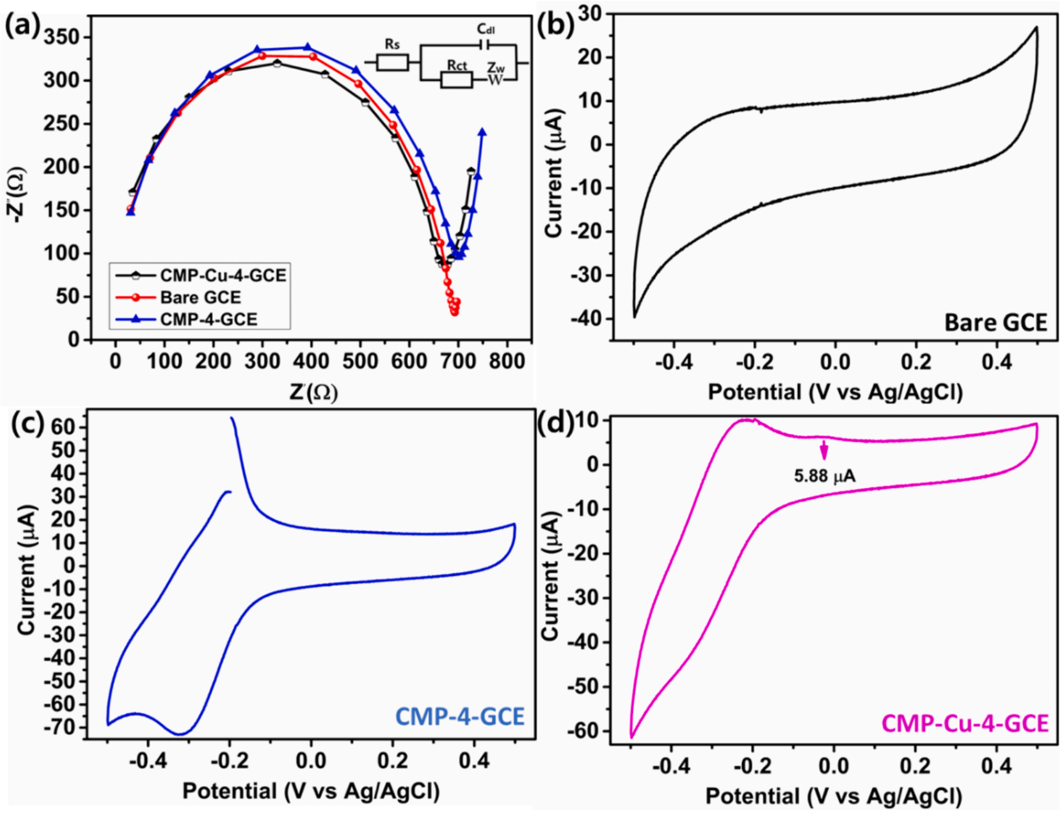

Fig. 4. **(a):** Impedance spectra of various modified GCEs and **(b-d)** CV response of Bare, CMP-4, and CMP-Cu-4 modified GCEs towards 500 nM DA.

Furthermore, the weak Lewis basic property of DA enhances the adsorption on the modified GCE.

A capacitance curve for bare GCE, CMP-4-GCE, and CMP-Cu-4-GCE was observed in the PBS (1 mM). The Cu-GCE demonstrated a double charge transfer mechanism at the same conditions (Fig. S6). The peak at −0.2 V is due to the oxidation of Cu° to Cu^+ on the Cu-GCE[38]. The presence of a second cathodic peak at −0.3 V indicates that a portion of Cu^+ is reduced back to its zero-oxidation state at this potential. In the second cycle, in the presence of DA (500 nM), the remaining Cu^+ ions on the Cu-GCE surface exhibit unresponsive behavior towards the analyte in the PBS solution, leading to a deviation in the CV plot from its typical pattern. The electrochemical response of bare GCE to 500 nM DA displays (Fig. 4b) anodic and cathodic plots that are unresponsive to the analyte. In contrast, CMP-4-GCE generates a highly unstable faradic peak at −0.18 V (Fig. 4c), indicating that the CMP-4-modified GCE is not sensitive to DA. However, the CV plots of CMP-Cu-4-GCE show an oxidation peak at −0.02 V and 5.88 μA (Fig. 4d), highlighting its superior electrochemical sensitivity compared to both bare GCE and CMP-4-GCE. This indicates that CMP-Cu-4-GCE exhibits superior sensitivity relative to other modified GCEs because of its advantageous surface adsorption characteristics. Analysis of the CV results from the CMP-Cu-4-GCE indicates that the DA redox peak current increases linearly with its concentration, ranging from 100 to 900 nM in 1 mM PBS-urine (Fig. 5). The anodic sensitivity ranges from 4.25 to 6.94 μA (R^2 = 0.9756), while the cathodic sensitivity ranges from −4.99 to −7.29 μA (R^2 = 0.9906) (Fig. S7a). The limit of detection (LOD) was determined from the plots of anodic and cathodic peak currents using formulas involving the standard deviation (Sy) and slope (S), yielding LOD values of 17.84 nM and 16.703 nM, respectively.

$$LOD = 3.3\frac{S_y}{S} \quad (1)$$

The specific capacitance (Csp) measurement assesses the CMP-Cu-4-modified glassy carbon electrode's capacity to store electrical charge per unit of surface area or mass. Mathematically Csp is defined as

$$Csp = Area\ of\ CV\ curve * scanrate * voltage\ window * mass \quad (2)$$

The area represents the integral of the CV curve (at a scan rate of 100 mV, (Fig. S7b)), the scan rate (V/s), the voltage window stands for the potential difference among the highest and lowest values, and the mass refers to the sample weight in grams. From the provided information, we calculated the specific capacitance (Csp) as 0.00115 μF/cm^2.

Double layer capacitance (Cdl) pertains to the capacitance occurring at the interface between the CMP-Cu-4-GCE and PBS-urine solution. Cdl is assessed from the gradient of the current density vs. scan rate plot, yielding a value of 0.5677 μF/g (Fig.S7c). ECSA represents the electrode surface area actively involved in the redox reaction. Mathematically, ECSA is defined as in Eq.3

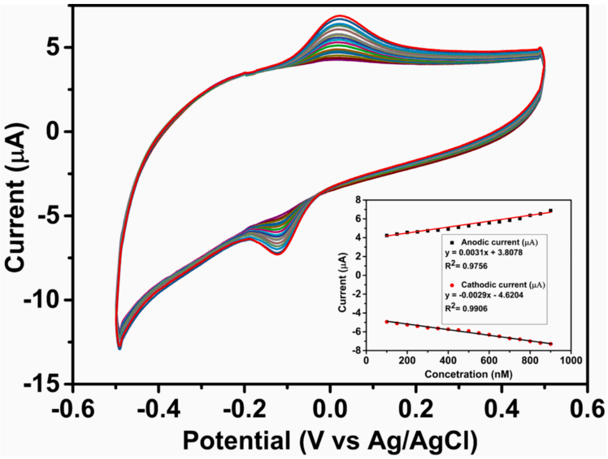

Fig. 5. CV plot for DA sensing from 100-900 nM.

$$ECSA = Cdl/Csp \quad (3)$$

As per the above equation, we calculated the ECAS as 493.65 cm^2/g.

The normalized current density (j_{norm}) for ECSA quantifies the reactive surface area of either an unmodified or modified GCE with diverse surfaces. The equation for J_{norm},

$$J_{norm} = j/ECSA \quad (4)$$

"j" represents the current density, while ECSA denotes the electrochemically active surface area. Based on the above equation we calculated the j_{norm} as 0.195 μA/g.

The scan rate (Fig. S7b) indicates the electric potential variation over time. The voltammetric response of 200 nM DA (1 mM PBS-urine, pH 7.4) was examined by varying the potential from 10 to 400 mV/s (Fig. S7b). The findings demonstrate that higher scan rates impact both the anodic and cathodic currents, causing a minor shift in the redox peak current due to the diffusion layer. Likewise, the kinetic characteristics of the CMP-Cu-4-GCE were investigated via the Log(A) vs. Log(scan rate) plot, confirming that Log(A) and Log(scan rate) adhere to a linear relationship (Fig.S7d).

$$y = 0.6551x - 0.4712 \quad (5)$$

The equation reveals a slope of 0.655, indicating that diffusion influences the DA detection mechanism through CMP-Cu-4-GCE.

Effect of pH on the redox mechanism

A pH of 7.4 is commonly identified as the physiological pH (ranging from 7.35 to 7.45) and is considered optimal for most biochemical reactions in human biological systems. Maintaining this pH range is essential for the effective functioning of these systems. Within this pH range, enzymes and both primary and secondary protein structures remain highly stable, which supports proper metabolic and cellular functions. We carried out CV experiments over a pH range from 7.4 to 6.5 to assess the electrochemical behavior of CMP-Cu-GCE in DA response, spanning from basic to acidic conditions, which includes the physiological pH range (7.35 to 7.45). The CMP-Cu-4-GCE exhibited its peak current response to DA (200 nM) at several pH values ranging from 7.4 to 6.5 in 1 mM PBS (Fig.S8(a)). As depicted in Fig. S8(b), a slight increase in peak current was observed when the pH values were reduced to 6.5, attributed to the specific adsorption facilitated by π-π interaction between dopamine and CMP-4.

Selective sensing of CMP-Cu-4-GCE towards DA over EP, NE, and AA

Two major interferences that impede the detection of DA in voltammetry are EP and NE. Since EP, DA, and NE all contain a catechol ring with differences only in the amine chain structures, their oxidation to quinone structure occurs simultaneously. To address this challenge, selectively adsorbing DA onto the modified electrode is the most effective approach. DA possesses a primary aminoethyl structure, whereas EP and NE have beta-hydroxy secondary and primary amine chains, making them more sterically hindered for adsorption on CMP-Cu-4-GCE (Scheme 2). Additionally, DA exhibits weaker Lewis basicity compared to EP due to its amine chain differences. Our team developed a composite comprising Cu^0 HT and CMP-4 for the selective sensing of DA. The soft–soft bonding between Cu^0 and DA enables the choosy sensing of DA over EP and NE. Moreover, the π-π interaction between the catechol ring and benzene group in CMP-4 enhances the adsorption of DA onto the CMP-Cu-4 surface. The slope (Eq. (5) derived from Log(A) and Log(scan rate) is 0.655, affirming that adsorption dominates in the DA detection mechanism in CMP-Cu-4-GCE. Following our analysis, we carried out an interference study using CMP-Cu-4-GCE in PBS, examining the effects of

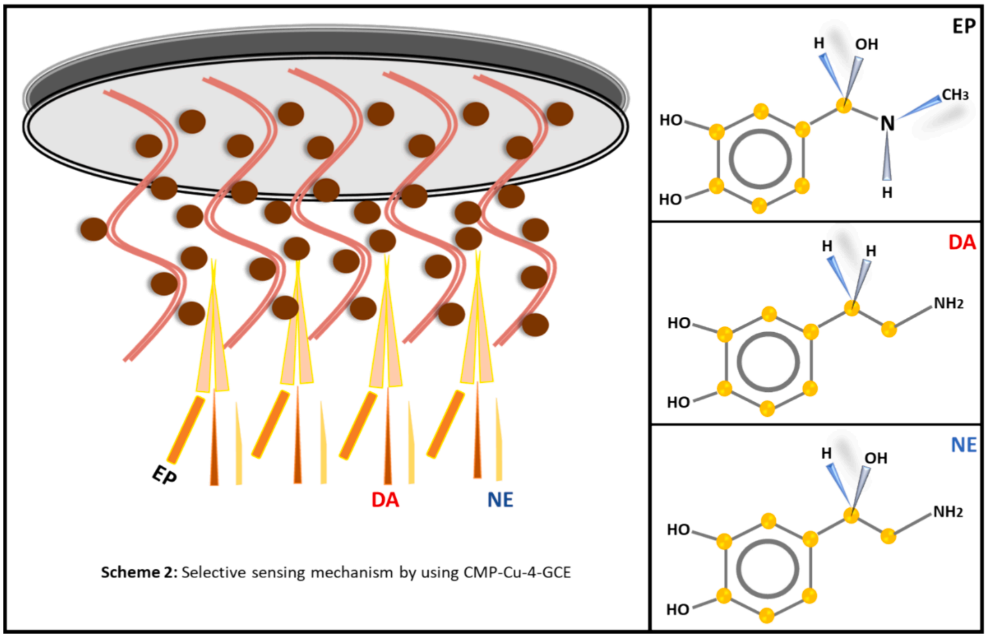

Scheme 2. Selective sensing mechanism by using CMP-Cu-4-GCE.

EP, NE, AA, uric acid (UA), lactic acid (LA), histidine (His), glutamic acid (GA), and gamma-aminobutyric acid (GABA) (Fig. S9 a&b). In the presence of these interferents, the CV plot only displays a peak at −0.2 V, which is attributed to the Faradaic current resulting from the oxidation and reduction processes involving CMP-Cu-4-GCE and the electrolyte. However, when DA is introduced into the PBS electrolyte, the analyte adsorbs onto the CMP-Cu-GCE surface, leading to characteristic redox peak currents of + 3.06 and −3.56 µA. Our findings revealed that CMP-Cu-4-GCE exhibited insensitive behavior towards interferents and demonstrated selective sensing towards DA. Additionally, we compared the performance of CMP-Cu-4-GCE with other modified GCEs, proving the selective sensing of our composite (Table 1).

Reproducibility, stability, and SPE experiments using CMP-Cu-4-GCE

Assessing the reproducibility and stability of the CMP-Cu-4-GCE is essential for practical applications. To gauge the stability of CMP-Cu-4-GCE, we conducted a CV analysis by repeating the experimental setup at a fixed DA concentration (800 nM, in PBS-urine). Upon analyzing the data, it was noted that the obtained CV result exhibited a consistent current response (Fig.S10(a)). The average and relative standard deviation (RSD) for the anodic current data were calculated from the data, amounting to 6.44 and 0.425 %, respectively (n = 8) (Fig.S10(b)). After conducting eight CV tests, we examined the morphological and compositional studies of CMP-Cu-4 on GCE. SEM-EDX analysis result after the stability test gives a consistent result with previous data, affirming the non-leachable and stable nature of the CMP-Cu-4 (Fig S11 and Table S2). Likewise, the reproducibility of the CMP-Cu-4-GCE was examined by fabricating the composite 3 times and assessing its CV response to dopamine (800 nM) (Fig.S12(a-c)). The consistent peaks observed in the CV plot validate the reproducibility of the findings. Additionally, we found the average and RSD as 6.45 and 1.23 %, respectively (Fig.S12(d)). To evaluate the life of the composite, we conducted a study using ethanol-dispersed CMP-Cu-4-nafion (0.5 mg in 1 ml), which was stored at −8°C for about one month (Fig.S13(a&b)). Our analysis showed that the composite was sensitive to a 700 nM DA solution, indicating that the CMP-4 and incorporated Cu NWs on the CMP surface remained intact and stable (Fig(S13(c)). Monitoring DA using screen-printed electrodes (SPE) is crucial for precision medicine in human health. Our group utilized an SPE with gold (Au) as the working electrode, platinum (Pt) as the counter electrode, and silver (Ag) as the reference electrode. The CMP-Cu-4-SPE was employed for DA detection using differential pulse voltammetry (DPV). The DPV plot of CMP-Cu-4-SPE for 0 nM DA exhibits a lack of sensitivity (Fig. S14a). Analysis of DPV data from the CMP-Cu-4-SPE reveals that the DA oxidation peak current increases linearly with concentration, ranging from 100 to 800 nM in 1 mM PBS-urine (Fig. S14b). The current sensitivity varies between 197.12 and 250.4 µA (R^2 = 0.9954) (Fig. S14b&c). The baseline inconsistency is attributed to the operational condition of the screen-printed electrode. After each cycle, a black residue accumulates on the platinum counter electrode due to the deposition of polydopamine. The LOD for DA sensing using CMP-Cu-4-SPE was determined using Eqn. (1) as 81.8 nM.

Table 1
Comparison of CMP-Cu-4-GCE with other modified electrodes.

Material	Technique	Linear range (µM)	LOD (µM)	Refs.
MOF-525-PEDOT NTs	DPV	2–270	0.04	[39]
Ce-MOF-808	AMP	20–200	1.3	[40]
Au@ZIF-8	DPV	0.1–50	0.01	[41]
SO3-MOF-808/GO	DPV	50–500	2.3	[42]
Cu-Co(2-MeIm) MOF@CNF//GCE	DPV	5.0–800	44.2	[43]
HKUST-1/GCE	DPV	12.5–175	0.11	[44]
GCE/Au-Cu_2O/rGO	DPV	10–90	3.9	[45]
PDA-RGO/Au	LSV	5–100	3.2	[46]
PyC	CV, DPV	18–270	2.3	[47]
Pdots@AMP-Cu	Fluorescence	10–400	4	[48]
WS_2 QDs	Fluorescence	5–50	3.3	[49]
I_2-CMP-CNT-4	CV, DPV	1–20	1, 1.7	[27]
Ag@MPBA-ABCDE	Fluorescence	5–50	5.9	[50]
CMP-Cu-4-GCE	CV	0.1–0.9	0.017 & 0.016	This work

Conclusion

In this study, we utilized a solvothermal synthesis technique to fabricate a weak-crystalline, conjugated microporous poly(arylene-ethynylene)-4 nanocomposite incorporating CuHT. The resulting CMP-Cu-4 exhibited a significant increase in both anodic and cathodic peak currents, indicating its potential as an electrochemical sensor for the rapid detection of DA. The composite's structure enhances dopamine adsorption and facilitates electron mobility between the GCE and analyte, resulting in a substantial improvement in electron transfer rate compared to a bare GCE. Moreover, this synthesis approach offers cost-effectiveness, rendering it an attractive option for developing DA sensing probes. The developed probe demonstrates outstanding selectivity, sensitivity, stability, and reproducibility, with a detection limit in the nanomolar range based on CV. The results suggest that DA voltammetry sensing is influenced by the analyte's adsorption on the CMP-Cu-4-GCE surface through aromatic functionality, soft–soft interactions, Lewis's basic nature, and steric hindrance. The peak current exhibited a linear correlation with DA concentrations ranging from 100 to 900 nM, with LODs of 17.84 and 16.03 nM ($R^2 = 0.9906$). Additionally, experiments indicated that EP, NE, and other interferents showed minimal response on the CMP-Cu-4-GCE in the presence of DA, highlighting its exceptional sensitivity, stability, selectivity, and reproducibility in DA detection. The DPV results using CMP-Cu-4-SPE indicate that it is a promising electrochemical probe for detecting DA in a PBS-urine solvent.

CRediT authorship contribution statement

Jose Paul: Writing – review & editing, Writing – original draft, Visualization, Validation, Supervision, Software, Project administration, Methodology, Investigation, Formal analysis, Data curation, Conceptualization. **Jongsung Kim:** Writing – review & editing, Supervision, Software, Resources, Project administration, Methodology, Investigation, Funding acquisition, Formal analysis.

Declaration of competing interest

The authors declare that they have no known competing financial interests or personal relationships that could have appeared to influence the work reported in this paper.

Acknowledgments

1) This research was supported by the Core Research Institute Basic Science Research Program through the National Research Foundation of Korea (NRF) funded by the Ministry of Education (2021R1A6A1A03038996), 2) National Research Foundation of Korea (NRF) grant-funded by the Korea government (MSIT) (NRF-2022R1A2C1009968), and 3) Gachon University research fund of 2021 (GCU-202106520001). We thank the Smart Materials Research Center for IoT at Gachon University for their technical support with instruments (FT-IR and SEM).

Appendix A. Supplementary data

Supplementary data to this article can be found online at https://doi.org/10.1016/j.jiec.2024.09.023.

References

[1] K.T. Ngo, E.L. Varner, A.C. Michael, S.G. Weber, ACS Chem. Neurosci. 8 (2) (2017) 329–338, https://doi.org/10.1021/acschemneuro.6b00383.
[2] M. Yang, L. Wang, H. Lu, Q. Dong, Micromachines 14 (2023) 5, https://doi.org/10.3390/mi14051088.
[3] C. Yang, M.E. Denno, P. Pyakurel, B.J. Venton, Anal. Chim. Acta 887 (2015) 17–37, https://doi.org/10.1016/j.aca.2015.05.049.
[4] X. Song, B. Han, X. Yu, W. Hu, Chem. Phys. 528 (2020), https://doi.org/10.1016/j.chemphys.2019.110514.
[5] L.S. Xie, G. Skorupskii, M. Dincă, Chem. Rev. (2020) 8536–8580, https://doi.org/10.1021/acs.chemrev.9b00766.
[6] T.C. Narayan, T. Miyakai, S. Seki, M. Dincă, J. Am. Chem. Soc. 134 (31) (2012) 12932–12935, https://doi.org/10.1021/ja3059827.
[7] J. Paul, J. Kim, Appl., Surf. Sci. 613 (December 2022) (2023) 156103, https://doi.org/10.1016/j.apsusc.2022.156103.
[8] J. Paul, R. Sangubotla, J. Kim, Electrochim. Acta 479 (January) (2024) 143885, https://doi.org/10.1016/j.electacta.2024.143885.
[9] E. Martínez-periñán, M. Martínez-fernández, J.L. Segura, E. Lorenzo, Sensors (2022), https://doi.org/10.3390/s22134758.
[10] P.V. Vaishag, S.A. Mohandas, M. Mufeeda, P. Gangadharan, P.A. Rasheed, ACS Sustain. Chem. Eng. 11 (34) (2023) 12771–12779, https://doi.org/10.1021/acssuschemeng.3c03173.
[11] M. Ankitha, F. Shamsheera, P.A. Rasheed, ACS Appl. Electron. Mater. (2023), https://doi.org/10.1021/acsaelm.3c01668.
[12] J.S.M. Lee, A.I. Cooper, Chem. Rev. 120 (4) (2020) 2171–2214, https://doi.org/10.1021/acs.chemrev.9b00399.
[13] J.-X. Jiang, F. Su, A. Trewin, C.D. Wood, N.L. Campbell, H. Niu, C. Dickinson, A.Y. Ganin, M.J. Rosseinsky, Y.Z. Khimyak, A.I. Cooper, Conjugated Microporous Poly (aryleneethynylene) Networks, n.d.
[14] S.K. Das, A. Chowdhury, K. Bhunia, A. Ghosh, D. Chakraborty, M. Das, U. Kayal, A. Modak, D. Pradhan, A. Bhaumik, Electrochim. Acta 459 (May) (2023) 142553, https://doi.org/10.1016/j.electacta.2023.142553.
[15] R. Rubio, M.B. Suarez, M.E. Pérez, D.A. Heredia, G.M. Morales, E.N. Durantini, L. Otero, M. Gervaldo, J.E. Durantini, Electrochim. Acta 458 (December 2022) 2023, https://doi.org/10.1016/j.electacta.2023.142552.
[16] J. Huang, X. Zhou, A. Lamprou, F. Maya, F. Svec, S.R. Turner, Chem. Mater. 27 (21) (2015) 7388–7394, https://doi.org/10.1021/acs.chemmater.5b03114.
[17] L. Chen, Y. Yang, D. Jiang, J. Am. Chem. Soc. 132 (26) (2010) 9138–9143, https://doi.org/10.1021/ja1028556.
[18] J.X. Jiang, A. Trewin, D.J. Adams, A.I. Cooper, Chem. Sci. 2 (9) (2011) 1777–1781, https://doi.org/10.1039/c1sc00329a.
[19] X. Liu, Y. Xu, D. Jiang, J. Am. Chem. Soc. 134 (21) (2012) 8738–8741, https://doi.org/10.1021/ja303448r.
[20] K. Zhang, D. Kopetzki, P.H. Seeberger, M. Antonietti, F. Vilela, Angew. Chemie - Int. Ed. 52 (5) (2013) 1432–1436, https://doi.org/10.1002/anie.201207163.
[21] Y. Xu, L. Chen, Z. Guo, A. Nagai, D. Jiang, J. Am. Chem. Soc. (2011) 17622–17625.
[22] J.L. Novotney, W.R. Dichtel, ACS Macro Lett. 2 (5) (2013) 423–426, https://doi.org/10.1021/mz4000249.
[23] P. Huang, J. Du, S.S. Gunathilake, E.A. Rainbolt, J.W. Murphy, K.T. Black, D. Barrera, J.W.P. Hsu, B.E. Gnade, M.C. Stefan, M.C. Biewer, J. Mater. Chem. A 3 (13) (2015) 6980–6989, https://doi.org/10.1039/c5ta00936g.
[24] S. Wan, F. Gándara, A. Asano, H. Furukawa, A. Saeki, S.K. Dey, L. Liao, M. W. Ambrogio, Y.Y. Botros, X. Duan, S. Seki, J.F. Stoddart, O.M. Yaghi, Chem. Mater. 23 (18) (2011) 4094–4097, https://doi.org/10.1021/cm201140r.
[25] S. Chen, B. Yuan, G. Liu, D. Zhang, Front. Chem. (2020), https://doi.org/10.3389/fchem.2020.601044.
[26] R. Gutzler, D.F. Perepichka, J. Am. Chem. Soc. 135 (44) (2013) 16585–16594, https://doi.org/10.1021/ja408355p.
[27] J. Paul, M. Moniruzzaman, J. Kim, Biosensors 13 (2023) 3, https://doi.org/10.3390/bios13030308.
[28] T.M. Geng, H. Zhu, W. Song, F. Zhu, Y. Wang, J. Mater. Sci. 51 (8) (2016) 4104–4114, https://doi.org/10.1007/s10853-016-9732-y.
[29] Z. Li, H. Li, H. Xia, X. Ding, X. Luo, X. Liu, Y. Mu, Chem. - A Eur. J. 21 (48) (2015) 17355–17362, https://doi.org/10.1002/chem.201502241.
[30] M. Akin, R. Bayat, M. Bekmezci, Z.K. Coguplugil, F. Sen, M. Baghayeri, A. Kaffash, F. Tehranejad-Javazmi, I. Sheikhshoaie, Carbon Lett. 33 (7) (2023) 1993–2001, https://doi.org/10.1007/s42823-023-00537-9.
[31] S. Tang, A. Liang, M. Liu, W. Wang, F. Zhang, A. Luo, Carbon Lett. 33 (7) (2023) 2129–2139, https://doi.org/10.1007/s42823-023-00556-6.
[32] Z. liang Liu, Y. Li, X. Guo, J. jie Tao, J. ning Huang, L. lin Fang, Carbon Lett. 33(6) (2023) 1549–59. 10.1007/s42823-023-00514-2.
[33] A.T.E. Vilian, S. An, S.R. Choe, C.H. Kwak, Y.S. Huh, J. Lee, Y.K. Han, Biosens. Bioelectron. 86 (2016) 122–128, https://doi.org/10.1016/j.bios.2016.06.022.
[34] H.J. Yang, S.Y. He, H.Y. Tuan, Langmuir 30 (2) (2014) 602–610, https://doi.org/10.1021/la4036198.
[35] F. Fathi, B. Sueoka, F. Zhao, X. Zeng, Anal. Chem. 95 (11) (2023) 4855–4862, https://doi.org/10.1021/acs.analchem.2c03609.
[36] J.C. Hidalgo-Acosta, A.M. Jaramillo, M.T. Cortés, Electrochim. Acta 359 (2020) 136932, https://doi.org/10.1016/j.electacta.2020.136932.
[37] Y. Deng, J. Zhao, Y. Yu, J. Gao, S. Zhao, J. Yuan, Q. Han, G. Cui, New J. Chem. 47 (27) (2023) 12759–12769, https://doi.org/10.1039/d3nj01376f.
[38] S.D. Giri, A. Sarkar, J. Electrochem. Soc. 163 (3) (2016) H252–H259, https://doi.org/10.1149/2.0071605jes.
[39] T.Y. Huang, C.W. Kung, Y. Te Liao, S.Y. Kao, M. Cheng, T.H. Chang, J. Henzie, H. R. Alamri, Z.A. Alothman, Y. Yamauchi, K.C. Ho, K.C.W. Wu, Adv. Sci. 4 (11) (2017) 1–8, https://doi.org/10.1002/advs.201700261.
[40] Y.T. Chiang, Y.J. Gu, Y. Da Song, Y.C. Wang, C.W. Kung, Electrochem. Commun. 135 (January) (2022) 107206, https://doi.org/10.1016/j.elecom.2022.107206.
[41] S. Lu, M. Hummel, K. Chen, Y. Zhou, S. Kang, Z. Gu, Electrochem. Commun. 114 (March) (2020) 106715, https://doi.org/10.1016/j.elecom.2020.106715.
[42] C.H. Shen, Y.N. Chang, Y.L. Chen, C.W. Kung, ACS Mater. Lett. 5 (7) (2023) 1938–1943, https://doi.org/10.1021/acsmaterialslett.3c00389.
[43] M. Wasi Ahmad, B. Dey, B.H. Kim, G. Sarkhel, D.J. Yang, S.K. Safdar Hossain, T. Kamal, A. Choudhury, Microchem. J. 193 (June) (2023) 109074, https://doi.org/10.1016/j.microc.2023.109074.
[44] F.A. Sofi, M.A. Bhat, K. Majid, New J. Chem. 43 (7) (2019) 3119–3127, https://doi.org/10.1039/c8nj06224b.
[45] T.K. Aparna, R. Sivasubramanian, M.A. Dar, J. Alloys Compd. 741 (2018) 1130–1141, https://doi.org/10.1016/j.jallcom.2018.01.205.
[46] K.N. Kudin, B. Ozbas, H.C. Schniepp, R.K. Prud'homme, I.A. Aksay, R. Car, Nano Lett. 8 (1) (2008) 36–41, https://doi.org/10.1021/nl071822y.

[47] G.P. Keeley, N. McEvoy, H. Nolan, S. Kumar, E. Rezvani, M. Holzinger, S. Cosnier, G.S. Duesberg, Anal. Methods 4 (7) (2012) 2048–2053, https://doi.org/10.1039/c2ay25156f.

[48] H. Huang, J. Bai, J. Li, L. Lei, W. Zhang, S. Yan, Y. Li, Anal. Bioanal. Chem. 412 (22) (2020) 5291–5297, https://doi.org/10.1007/s00216-020-02742-1.

[49] X. Zhao, D. He, Y. Wang, C. Fu, Mater. Chem. Phys. 207 (2018) 130–134, https://doi.org/10.1016/j.matchemphys.2017.12.045.

[50] P. Sivakumar, S. Priyatharshni, K. Kumar, Mater. Chem. Phys. 240 (June 2019) (2020) 122167, https://doi.org/10.1016/j.matchemphys.2019.122167.